Ex Vivo Evaluation of a Minimally Invasive Approach for Cochlear Implant Surgery

Thomas S. Rau, Samuel John, Marcel Kluge, Felix Repp, M. Geraldine Zuniga, Jan Stieghorst, Max E. Timm, Max Fröhlich, Omid Majdani, and Thomas Lenarz

***Abstract*—*Objectives:* Drilling a minimally invasive access to the inner ear is a demanding task in which a computer-assisted surgical system can support the surgeon. Herein, we describe the design of a new microstereotactic targeting system dedicated to cochlear implant (CI) surgery and its experimental evaluation in an ex vivo study. *Methods:* The proposed system consists of a reusable, bone-anchored reference frame, and a patient-specific drilling jig on top of it. Individualization of the jig is simplified to a single counterbored hole drilled out of a blank. For accurate counterboring, the setup includes a manufacturing device for individual positioning of the blank. The system was tested in a preclinical setting using twelve human cadaver donors. Cone beam computed tomograph (CBCT) scans were obtained and a drilling trajectory was planned pointing towards the basal part of the cochlea. The surgical drill was moved forward manually and slowly while the jig constrained the drill along the predetermined path. *Results:* Drilling could be performed with preservation of facial nerve in all specimens. The mean error caused by the system at the target point in front of the cochlea was 0.30 mm $\pm$ 0.11 mm including an inaccuracy of 0.09 mm $\pm$ 0.03 mm for counterboring the guiding aperture into the jig. *Conclusion:* Feasibility of the proposed system to perform a minimally invasive posterior tympanotomy approach was shown successfully in all specimens. *Significance:* First evaluation of the new system in a comprehensive ex vivo study demonstrating sufficient accuracy and the feasibility of the whole concept.**

***Index Terms*—Direct cochlear access, minimally invasive, drilling accuracy, image-guided surgery, microstereotactic frame.**

Manuscript received 28 February 2022; revised 3 June 2022; accepted 14 July 2022. Date of publication 8 August 2022; date of current version 26 December 2022. This work was supported in part by the Federal Ministry of Education and Research of Germany (BMBF) under Grants 13GW0019A/C/E, 13GW0367B, and 13GW0265A, in part by German Research Foundation (DFG) through Germany's Excellence Strategy – EXC 2177/1 – Project under Grant 390895286, in part by European Union (EFRE), and in part by Lower Saxony (SER) ZW 3-85031593. Electrode arrays have been provided by MED-EL. *(Corresponding author: Thomas S. Rau.)*

Thomas S. Rau is with the Department of Otolaryngology and Cluster of Excellence EXC 2177/1 "Hearing4all", Hannover Medical School, 30625 Hannover, Germany (e-mail: rau.thomas@mh-hannover.de).

Samuel John, Marcel Kluge, Felix Repp, and Jan Stieghorst are with the OtoJig GmbH, Germany.

M. Geraldine Zuniga, Max E. Timm, Omid Majdani, and Thomas Lenarz are with the Department of Otolaryngology and Cluster of Excellence EXC 2177/1 "Hearing4all", Hannover Medical School, Germany.

Max Fröhlich is with the MED-EL Medical Electronics GmbH, MED-EL Research Center, Germany, and also with the Department of Otolaryngology, Hannover Medical School, Germany.

This article has supplementary downloadable material available at https://doi.org/10.1109/TBME.2022.3192144, provided by the authors.

Digital Object Identifier 10.1109/TBME.2022.3192144

I. Introduction

A COCHLEAR implant (CI) is a well-established intervention to restore hearing in patients who are deaf or suffering from severe-to-profound hearing loss. The implantable part of the CI system consists of a stimulator/receiver and an electrode array (EA). Surgical access to the cochlea is required to place the EA into the scala tympani (ST) and then enable electric stimulation of the auditory nerve. The conventional approach involves drilling a mastoidectomy followed by posterior tympanotomy passing through the facial recess—a narrow gap between the facial nerve (FN) and the chorda tympani (ChT). Although the EA is very thin (typically less than 1.3 mm in diameter), drilling of the mastoid cavity means removal of a comparable large amount of bone to identify anatomic landmarks that guide surgeons through the lateral skull base to the cochlea. This large surgical exposure costs time, may increase risk of injury, and requires specially trained surgeons.

Replacing the conventional approach with a less invasive procedure where the amount of bone removal is reduced almost to the diameter of the EA could be beneficial in many ways. Additionally, the increasing demand for CIs secondary to the expansion of the indication criteria and the rapid increase of the aging population globally urges a significant simplification of CI surgery. Furthermore, simplifying CI surgery using a preplanned trajectory based on the individual anatomy could help improve structure preservation in patients with residual hearing [1]–[3].

The vision of minimally invasive CI surgery (minCIS; a.k.a. percutaneous cochlear implantation, PCI) aims to drill just a single path to enter the cochlea. The pioneer in this field, Dr. Robert Labadie (Vanderbilt University Medical Center, Nashville, Tennessee), first described this idea [4]. Since then several concepts of surgical assistance devices have been described in order to simplify the surgical procedure; to improve precision of EA insertion for better hearing preservation; to reduce OR time; and to decrease the costs of the procedure while keeping today's high safety standards and low failure rate of the conventional CI surgery [5], [6].

This work is licensed under a Creative Commons Attribution 4.0 License. For more information, see https://creativecommons.org/licenses/by/4.0/

Such concepts can be roughly classified into 1) frame-less approaches, where an integrated image-guided surgery (IGS) system tracks the surgical instruments and provides the necessary spatial information to move the drill a long a previously planned trajectory, and 2) stereotactic approaches, where an individually adjusted or fabricated instrument guide is rigidly attached to the skull, thereby maintaining the drill along the desired trajectory. Note that hand-held use of a tracked otologic drill was originally tested [4], [7] but later discarded due to difficult use and insufficiently safe utilization [8], [9]. To overcome the limitations of human ability to translate 3D visualizations of an IGS into hand movements that precisely follow the planned trajectory, robots have been incorporated in the workflow [9]–[12]. The most prominent example is the HEARO robot developed in Bern (CAScination AG, Bern, Switzerland) [13], [14] which became the first assistant device for minCIS that received CE mark approval.

The second category includes several concepts of micro-stereotactic frames (MSF), which are bone-anchored, rigid instrument guides, a.k.a. surgical targeting systems. Here, a custom drilling jig restricts the surgical instrument to be moved along a straight path which fits to the previously defined trajectory. In all MSF, rigid fixation to the target structure is enabled using screw-in bone-anchors with customized component mounted on top of them. This individualized jig is designed based on the location of the anchors and the desired trajectory. Different concepts of manufacturing have been described including 3D printing (e.g., the StarFix [8], [15]), milling on a computer-numeric-control (CNC) machine (e.g., the Microtable [16]–[18], or biopsy guides [19]), by individual setting the lengths of three to six struts [20], [21], or by sticking prefabricated parts together (e.g., the GluingJig system [22], or the Freeze Frame [23]).

3D printing however, requires hours and causes a delay of several hours [16], [24]. This delay needs a separate surgical intervention only for the bone-anchor implantation prior to imaging, which additionally burdens the patient [16], [24]. Therefore, enabling the whole procedure to be performed in a single surgery was the motivation for the Vanderbilt group to develop the so-called Microtable [17]. For that, the geometry of the surgical template is much simpler and so it does not require cumbersome printing of the whole volume by adding layer by layer in a patient-specific manner. Instead, fabrication of the Microtable is reduced to four counterbore holes which need to be drilled out of a blank with specified depths and locations. Evidently, removing only parts of whole volume by milling is much faster (a.k.a. subtractive rapid prototyping [19]). The microtable can be milled using an automated CNC machine in approx. 6-15 min [16], [17]. After adding prefabricated legs, the whole assembly needs to be sterilized to enable its use under sterile conditions. Following the idea of the inventors, flash sterilization will be utilized. However, this adds extra time to the surgery [16].

The development of the proposed system was motivated by the aim to provide a method that allows individualization of the MSF under sterile conditions. Therefore, individualization of the jig was simplified to a single counterbored hole (Fig. 1) which needs to be drilled out of a blank [25]—a procedure which shall be performed under aseptic conditions in a manufacturing system as described below. The customized jig fits on top of a reusable, bone-anchored reference frame, which serves both for rigid bone-anchorage and image registration.

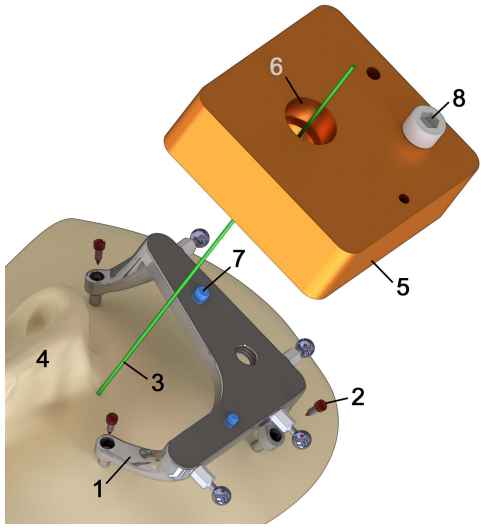

Fig. 1. Schematic drawing of the micro-stereotactic surgical targeting system. It includes a unique, bone-anchored reference frame (1), fixed by three bone screws (2) near to the roughly estimated drilling trajectory (3) behind the ear (4), as well as an individually fabricated jig (5). A counterbore hole (6) serves a guidance aperture that constrains the surgical tool along the planned trajectory. Dowel pins (7) for a clearance-free connection and its locking with a screw (8).

Herein we present the first experimental evaluation of the system and its accuracy in a preclinical setting using full body human cadaver donors. In contrast to a previous conference paper [25] not only preliminary but full results of the study including all twelve donors are presented. This study aims to a) determine the feasibility of our system to drill through the facial recess without unexpected damages to vital structures, b) estimate the system's accuracy to drill in the irregular mastoid bone, and c) to collect practical experience and surgical feedback for the further development of hardware and software and the surgical concept.

II. Material and Methods

First, the proposed minCIS targeting system and the ex vivo study are described. Then the methods used to evaluate the system's accuracy are reported.

A. Surgical Procedure

1) Specimen Preparation: Twelve anonymized, full-body human cadaver donors were used for preclinical evaluation of the targeting system. The human bodies were used under the ethics approval (A 2016-0083, University of Rostock, Germany). All specimens were Thiel-fixed; a method developed to preserve the natural plasticity and flexibility of the soft tissues with better similarity to a fresh specimen when compared with formalin-based embalming techniques [26].

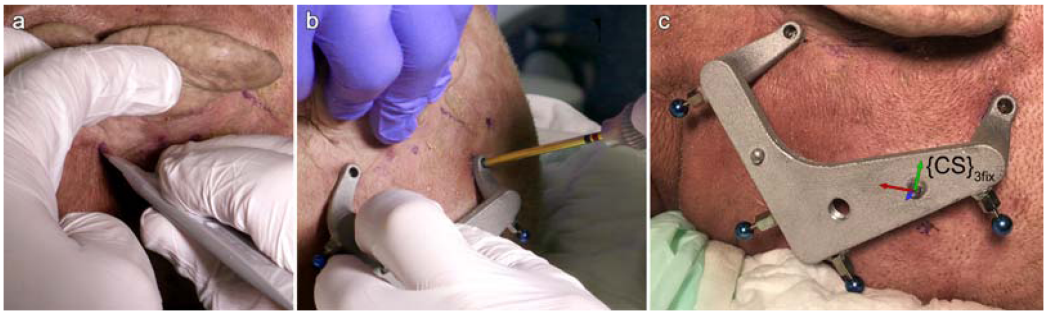

Fig. 2. The reference frame is fixed behind the pinna through small skin incisions (a) and bone-anchored using three screws (b). It serves as a rigid connection to the skull and will carry the individual jig mounted on top using two dowel pins and a screw. (c) The reference frame provides four fiducial for image-to-patient registration. This transferred a common coordinate system (CS) from physical into image space.

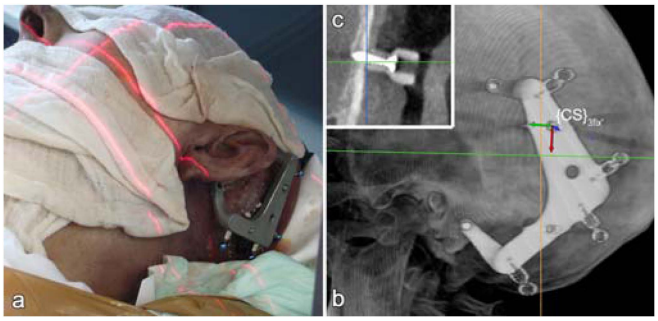

Fig. 3. (a) Imaging of the head with attached reference frame using a mobile CBCT scanner. The red laser lines indicate the image volume. (b) The visible frame enables mapping of the image space to patient space. (c) Proper placement of all bone screws can be verified.

First, a reusable reference frame was fixed to the skull behind the left ear (Fig. 2, mirrored version necessary for right ears). Due to its design and the selected method of bone fixation by three separate bone screws, it is referred to as "Trifix" in the following. The position for the Trifix was chosen by the surgeon based on the roughly estimated course of the desired drilling. Three small skin incisions (Fig. 2(a)) enable direct contact of the frame with the skull. Three self-drilling and self-tapping bone screws (Max Drive Drill Free 2.0 × 9, KLS Martin Group, Tuttlingen, Germany and EASYLINE CMF bone screw 20-712-11 2,0x11, General Implants GmbH, Villingen-Schwenningen, Germany) were used to ensure solid bone-anchorage (Fig. 2(b)). The design of the countersunk holes at the end of the Trifix's legs limits screw-in depth to 3.6 mm. Fig. 2(c) shows the Trifix including four titanium spheres added to the frame for image-to-patient registration. Two dowel pins protruding from the planar top surface of the reference frame enables precise mounting of the individual jig with negligible clearance. A metric thread (M6) in the Trifix is used to secure the connection.

2) Imaging: Afterwards, a mobile, intraoperative cone beam computed tomograph (CBCT, xCAT, Xoran, Ann Arbor, MI, USA) was utilized for image acquisition (Fig. 3). All images were captured with an isotropic voxel size of 0.3 mm. Then, the images of the scan were examined to visually confirm proper bone fixation (Fig. 3(c)) and identification of the entire Trifix (Fig. 3(b)). The visible region should include all four spherical registration markers. When insufficient bone-anchorage was detected, the position of the Trifix was slightly changed to improve the fitting of the affected screw and an additional scan was conducted.

3) Planning: As the next step, image data was transferred to a notebook running our custom-made planning software. It is a plugin, written in Python 2.7 (Python Software Foundation, Delaware, USA), for the open source software 3DSlicer (version 4.8.1) [27]. The plugin includes extensions for manual selection of the spheres as well as path planning (Fig. 4). The latter allowed for manual definition, inspection, and manipulation of an access path from the skull surface to a target region. The different diameters of the drill bit were visualized in 3D and as an outline in the traditionally slice views (Fig. 4(b)). Using the interactive graphical user interface provided by the planning software, a trajectory was planned which starts at the lateral cranium and passes the facial recess with maximal safety margins (at least 0.3 mm as it is the resolution of the CBCT) to FN, ChT, ossicular chain, and external auditory canal, with giving more weight to the FN. In case #05 the ChT could not be identified due to insufficient image quality. Trajectories were planned to end in the middle ear close to the round window at target point $p_{t,plan}$ (Fig. 4(b)) pointing towards the basal part of the cochlea aiming for a tangential access to the inner ear, i.e., aligned with the basal turn. All trajectories were reviewed and approved by an experienced CI surgeon.

The selected positions of the titanium spheres were registered to the positions of the spheres in physical space measured prior to the intervention using a portable coordinate measuring machine (CMM, Romer Absolute Arm Compact 7312, Hexagon Manufacturing Intelligence, Wetzlar, Germany). The volumetric accuracy of the CMM is 0.025 mm. This registration step transferred the coordinate system defined by the Trifix to the image space where trajectory planning took place. Finally, coordinates of the target point ($p_{t,plan}$) and the entry point ($p_{e,plan}$) were saved in the Trifix coordinate system and exported for computation of the inverse kinematic of the manufacturing system.

4) Individualization of the Jig: To transfer the planned trajectory to the patient, the patient-specific counterbore hole for instrument guidance (referred to as "guidance aperture" in the following) needs to be drilled into the blank. As this

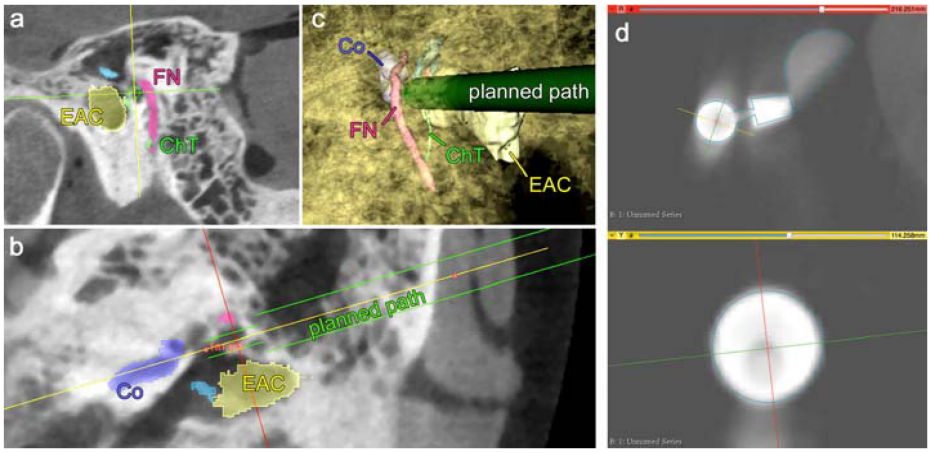

Fig. 4. (a)–(c) Screenshots of the 3DSlicer view of path planning with segmented anatomic structures (FN: Facial nerve, ChT: Chorda tympani, Co: Cochlea; EAC: External auditory canal). (a) and (b) Slice views cutting along the planned drill path. (c) 3D view. (d) Manually selected sphere marker of the MSF for registration of the planning to the patient.

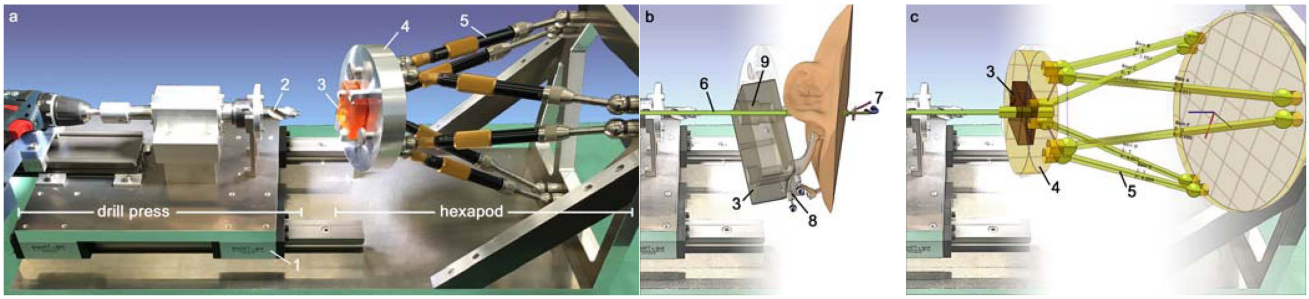

Fig. 5. (a) Overview of the manufacturing system. A linear sliding mechanism (1) enables manual pressing of the polymer drill bit (2) into a Ultem blank (3) for its customization. Position and orientation of the blank can be adjusted in a patient-specific manner by moving the upper platform (4) by means of adjusting the length of all six struts (5) of the hexapod. (b) A schematic drawing of the device illustrates the basic concept: the main axis (6) of the polymer drill bit represents the individually planned trajectory to the cochlea (7) while the blank is positioned in such a way that it fits to the specific position of the reference frame (8). In this individual configuration, the blank is finalized by adding a counterbore hole (9) Which later guides the instruments. (c) Custom software calculates and visualizes the patient-specific length of all six struts (5) of the hexapod by solving the inverse kinematic of the parallel manipulator.

is one of the most critical steps regarding overall accuracy, a manufacturing system was designed, produced, and used in this study (Fig. 5). It includes a passive Stewart-Gough-Platform (a.k.a. "Hexapod"), which serves for temporary positioning of a blank (Ultem 1000 resin, Arthur Krüger GmbH, Barsbüttel, Germany) during drilling of the counterbore hole (Ø 12.5 mm to 15.0 mm). The design of the manufacturing system was inspired by a guiding sleeve positioning system (X1med3D, Schick GmbH, Schemmerhofen, Germany) that belongs to the med3D procedure (med3D GmbH, Heidelberg, Germany) for template-guided dental implantations. The adjustable struts of the X1med3D were purchased solely while all other parts of the device have custom-made designs and were fabricated in the institution's own machine shop.

Temporary fixation of the blank to the moving platform of the manufacturing system is enabled using the identical mechanical coupling interface as available on the top surface of the Trifix. Individual orientation and position (pose) of the hexapod's moving platform was adjusted by manually setting the length of all six struts. Length values were calculated by a software that solves the inverse kinematic of the hexapod (Fig. 5(c), [28]), written in Python using the libraries NumPy and Plotly. As a result of pose setting, the Ultem blank was coaxially aligned to the planned trajectory represented by the main axis of a polymer drill bit. This is a custom-made stepped bit with a 12.5 mm diameter pilot and 15.0mm diameter counterbore. A cordless drill (GSR 10,8-2-LI, Robert Bosch Power Tools GmbH, Germany), mounted on linear slider, was used to drive the drill bit, working like a horizontal drill press. The blank was customized in a single shot process with approx. 400 rpm by manually advancing the drill until the step of the counterbore was roughly half-way in the jig.

5) Drilling: Afterwards the individualized jig was removed from the manufacturing system, cleaned, and equipped with a drill guide suited to a custom-made twisted step drill bit. The whole assembly was mounted onto the Trifix (Fig. 6). The shank and the basal part of the twisted drill bit was designed with 4.0 mm in diameter to increase its stiffness while the apical part is 1.8 mm in diameter to consider the narrow dimensions of

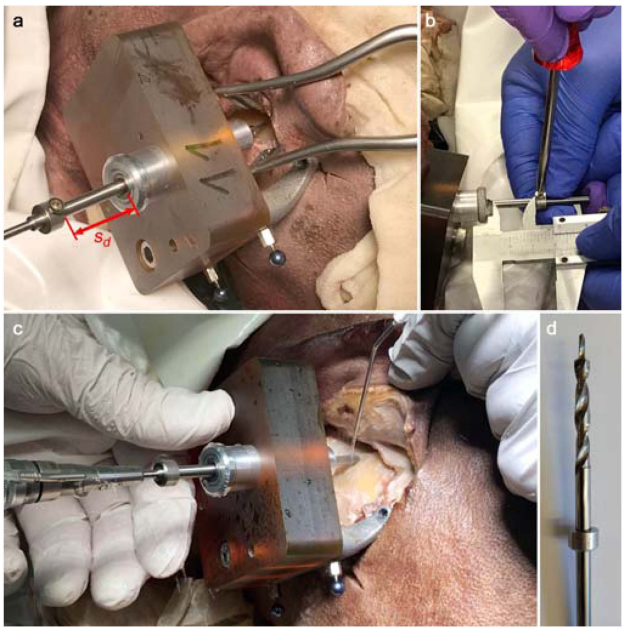

Fig. 6. (a) Individualized jig mounted to the Trifix with the drill guide and drill bit inserted. While placing the tip of the drill bit on the skull surface, the clearance (s_d) between the set collar and the drill bushing is equal to the possible drilling depth. (b) Adjustment of the position of the set collar to the desired drilling depth. (c) Drilling under continuous irrigation with water using a hand-held otological drill. (d) Close up image of the custom drill bit.

the facial recess [29]. The shank of the drill bit was equipped with a set collar for mechanical limitation of the drilling depth (Fig. 6(a), (b)). Individual drilling depth, in terms of distance between the skull surface and the target point $p_{t,plan}$, was measured during trajectory planning. Using the customized instrument guide, the access to the middle ear was drilled by the surgeon under continuous irrigation with water (Fig. 6(c)). Drilling was performed slowly in order to apply only slight thrust and was stopped when the set collar reached the upper end of the drill bushing.

B. Accuracy Evaluation

After drilling, a second CBCT scan was acquired to assess the system's accuracy. While the reference frame was kept in place, the jig was demounted from the Trifix to enable access to the drilled canal (Fig. 7(a)). The latter was flushed with water in order to remove remaining bone dust. Afterwards, a titanium rod, having the same outer diameters as the drill bit, was inserted (Fig. 7(b)) to improve visibility of the drilled canal in the CBCT scan (Fig. 7(c) and (d)). Imaging was used to assess the preservation of all critical structures. In some cases, were ChT or FN could hardly be identified, a conventional mastoidectomy was performed to visually assess the preservation of FN and ChT using the surgical microscope.

The total drilling error was determined using two different registration methods. The first one relied on intensity-based automatic image registration. Preoperative images (including the planned trajectory) and postoperative images (showing the titanium rod representing the actually drilled canal) have been

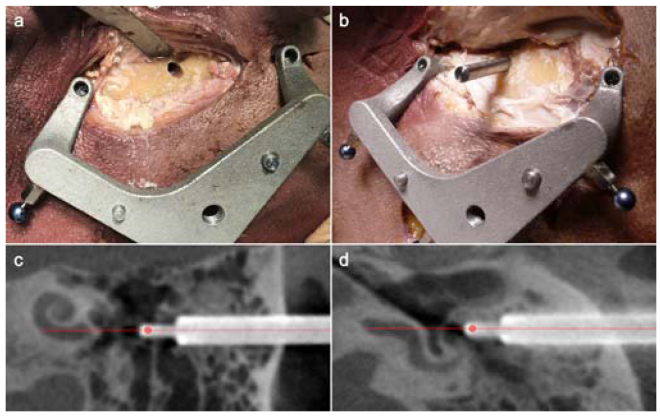

Fig. 7. (a) Entry of the drilled canal after removal of the jig. (b) Titanium rod inside the canal. (c) and (d) Exemplary images from a second CBCT scan showing the titanium rod which indicates the drill canal targeting the inner ear. Main axis is highlighted in red.

registered automatically (BRAINS fit module in 3D Slicer). For the second method, feature-based registration was conducted using the spherical marker attached to the Trifix. This approach replaces the uncertainty of the intensity-based image registration with the uncertainty of the sphere marker localization (a.k.a. fiducial localization error, FLE) [30].

The location of the titanium rod was determined manually by placing a virtual cylinder over the titanium rod for which our same 3D slicer module was used as already used for planning. The deviation between the planned trajectory and the main axis of the cylinder (representing the drilled canal), referred to as "total drilling error" (ε_{drill}) in the following was measured as the radial error on a plane perpendicular to the planned path at the level of $p_{t,plan}$ (cf. target positioning error (TPE)-lateral as described by [31]). The actual target points are denoted $p_{t,img}$ and $p_{t,fid}$ depending on the method used for registration of both CBCT scans (*img* denotes intensity-based image registration; *fid* denotes fiducials in case of the feature-based registration method). The corresponding total drilling error is referred to as ${}_{img}\varepsilon_{drill}$ and ${}_{fid}\varepsilon_{drill}$, respectively. Additionally, the angle between the planned trajectory and the axis of the cylinder model representing the titanium rod was computed (${}_{img}\Delta\theta_{drill}$ and ${}_{fid}\Delta\theta_{drill}$). Finally, the Euclidian 3D distance between the calculated target points when transformed via the two registration methods is reported as $\|p_{t,img} - p_{t,fid}\|$.

To provide further insights into the contribution of different effects to the determined total drilling error additional measurements of system components were conducted. First, the final length of all struts of the manufacturing system for each jig was measured (Romer Absolute Arm Compact 7312). Second, it was analyzed how accurate the guidance aperture can be drilled into the blank. Therefore, the main axis of the hole was measured using an optical coordinate measurement machine (XM-T1200, Keyence Deutschland GmbH, Neu-Isenburg, Germany) and compared to the planning, which is a measure for the error of the fabrication process of the jig. The error was extrapolated to the level of $p_{t,plan}$ and denoted as ${}_{CMM}\varepsilon_{jig}$ and ${}_{CMM}\Delta\theta_{jig}$ for the radial and angular deviation, respectively. Third, the

TABLE I
RESULTS OF ACCURACY EVALUATION

specimen	${}_{img}\varepsilon_{drill}$	${}_{fid}\varepsilon_{drill}$	${}_{CMM}\varepsilon_{jig}$	$\|p_{t,img} - p_{t,fid}\|$	${}_{img}\Delta\theta_{drill}$	${}_{fid}\Delta\theta_{drill}$	${}_{CMM}\Delta\theta_{jig}$
# 01	0.13	0.30	0.118	0.25	0.38	0.59	0.041
# 02[m]	0.19	0.28	0.095	0.46	0.96	0.81	0.003
# 03[h]	*0.91*	*0.88*	*1.043*	0.07	*0.10*	*0.05*	*0.120*
# 04	0.24	0.17	0.093	0.27	0.08	0.12	0.022
# 05[m]	0.44	0.32	0.068	0.18	0.40	0.30	0.030
# 06	0.25	0.28	0.077	0.09	0.31	0.43	0.005
# 07[f]	0.49	0.36	0.097	*0.42*	0.49	0.49	0.035
# 08[h]	*0.76*	*0.83*	*0.789*	0.21	*0.87*	*0.96*	*0.057*
# 09	0.35	0.33	0.138	0.19	0.40	0.33	0.005
# 10	0.31	0.13	0.044	0.26	0.34	0.13	0.000
# 11	0.22	0.09	0.113	0.14	0.16	0.40	0.025
# 12[f]	0.37	0.20	0.081	*0.55*	0.82	0.10	0.005
mean ± SD (technical system accuracy)	0.30 ± 0.11	0.24 ± 0.09	0.09 ± 0.03	0.21 ± 0.11	0.43 ± 0.27	0.37 ± 0.23	0.02 ± 0.03
mean ± SD (including all operating errors)	0.39 ± 0.23	0.35 ± 0.25	0.23 ± 0.33	0.26 ± 0.15	0.44 ± 0.30	0.39 ± 0.29	0.03 ± 0.03

Drilling errors ε in mm and angular deviation $\Delta\theta$ in degree as described in the text. $\|p_{t,img} - p_{t,fid}\|$ denotes the Euclidean distance at the target point p_t between the two registration methods. Superscripts in the specimen column indicate datasets where visible movement artifacts introduced problems for image registration (m), and an identified movement of the frame (f). The technical system accuracy was computed including all experiments, which were not compromised by a considerable human error (h). The last value for the column $\|p_{t,img} - p_{t,fid}\|$ contains all measurements but the ones with movement of the frame (f). *Excluded values are grayed out*. SD: standard deviation.

variations in the manual process of marking the titanium rod and the spherical markers were estimated. Therefore, five postexperimental scans were randomly selected in order to compare the performance of six people with varying experience in working with 3D data. Each participant was asked to fit a cylinder to the titanium rod in the images and repeat this procedure three times. Afterwards, the inter-individual and intra-individual performance was calculated. For each of the five patients, all 18 fitted cylinders were averaged. The uncertainty $\sigma(\varepsilon)$ was estimated at the target as the mean distance to the averaged cylinder, i.e., the standard deviation of the manual measurements. Similarly, the uncertainty $\sigma(\theta)$ of the angle and the uncertainty $\sigma(S)$ of manually locating the sphere markers of the frame was determined.

III. RESULTS

Feasibility of the minimally invasive posterior tympanotomy approach using our new micro-stereotactic targeting system was shown in all 12 specimens. The facial nerve was preserved in all cases; whereas chorda tympani was sacrificed as planned in one case as the preoperative imaging quality was insufficient for a reliable identification.

Mean accuracy of the whole micro-stereotactic targeting system for drilling along a planned trajectory, measured at the target point close to the cochlea, was ${}_{fid}\varepsilon_{drill} = 0.24$ mm $\pm$ 0.09 mm and ${}_{img}\varepsilon_{drill} = 0.30$ mm $\pm$ 0.11 mm when using the spherical markers or the intensity-based approach for image registration, respectively. Measurements of the counterbore hole in the jig projected to the target points resulted in ${}_{CMM}\varepsilon_{jig} = 0.09$ mm $\pm$ 0.03 mm on average. The drill guide fits very tight inside the guidance aperture without observable clearance. Therefore, we assume that this connection does not deteriorate the overall accuracy. Angular drilling errors were found to be ${}_{fid}\Delta\theta_{drill} = 0.37° \pm 0.23°$, ${}_{img}\Delta\theta_{drill} = 0.43° \pm 0.27°$, and ${}_{CMM}\Delta\theta_{jig} = 0.02° \pm 0.03°$. These values describe the technical accuracy as deduced from 10 of 12 cases.

In the other two cases, human error in operating the manual hexapod were observed whereby in each case the length of one leg was set considerably wrong due to a mistake of the operator. Despite the high drilling error, integrity of FN and ChT was confirmed by microscopic inspection (Supplementary Fig. S4). Table I summarizes the results from all 12 experiments.

Analyzing the repeated position determination of the rod (Sup. Figs. S1, S3) showed that the mean position of the rod within the CT scan can be determined to $\sigma(\varepsilon) = 0.11$ mm $\pm$ 0.02 mm, similar to the uncertainty of the registration spheres $\sigma(S) = 0.11$ mm $\pm$ 0.01 mm (Sup. Figs. S2, S3). The uncertainty of angle of the rod was $\sigma(\theta) = 0.24° \pm 0.06°$ (Sup. Fig. S3).

Insufficient bone-anchorage was detected in the images in three cases. This leads to re-fixation of the reference frame and repetition of the CBCT scan. An unusual thick skin flap was observed in one specimen which prevented sufficient fixation of the reference frame through the skin incision due to the too short length of the Trifix's legs (Fig. 1). In that case, a large retroauricular incision was required to enable rigid fixation. In one case (#4) only three spheres were visible in the post CT scan, which might influence registration accuracy with the image data used for trajectory planning.

IV. DISCUSSION

CI surgery conventionally requires large bone removal at the skull behind the ear—a procedure that has not undergone any noteworthy changes in the past decades—but goes along with several drawbacks [32]. Therefore, several groups are working on the vision of a minimally invasive approach to the inner ear and it is already shown that rigidly attached MSF [33], [34] as well as image-guided robot systems [13], [35] can provide sufficient accuracy. However, minCIS is far from being a well-established and widely used standard. Although the HEARO robot is sophisticated from a technological point of view, a task autonomous surgical robot may not be the optimal solution from an economic perspective [34].

Our research is focused on frame-based approaches, as we believe that the rigid fixation to the patient's skull is an inherent safety feature and allows for simpler and therefore more cost-efficient solutions. For MSF, the time required for custom fabrication of the surgical template impacts clinical implementation. Current drawback of "rapid" prototyping is the delay due to the time consuming production step as for the 3D-printed StarFix microTargeting platform [16], [24]. In case of the Microtable, whose geometry is simpler and therefore fabrication is much faster, the whole assembly needs to be sterilized afterwards to enable its use under sterile conditions. However, in a more recent clinical study using a commercial version of the Microtable concept, the CNC-supported fabrication was done at an external facility going back to the strategy of bone anchor placement as an outpatient treatment while the stereotactic surgery took place approximately one week later. The skin incision over bone-anchors was closed and re-opened at the day of the surgery [16]. This needs to be discussed in terms of patient comfort as it is known to cause pain [24] and inherent risk of infection. Nevertheless, the overall patient comfort will be better than with conventional frame-based stereotaxy for which significantly higher discomfort in comparison to an IGS without bone fixation was shown [36].

Development of our surgical targeting system was driven by the motivation to further simplify the patient specific fabrication of the jig in order to make it feasible during the surgery under sterile conditions. This was achieved by reducing complexity of the customization step. Now drilling of only one single counterbored hole out of a blank is necessary. Consequently, the jig can not be adapted to varying positions of separate bone anchors as it is implemented in the concept of the milled Microtable or the 3D printed STarFix. In contrast, the blank has to be prefabricated with a standardized coupling interface that fits to the bone anchored fixation system. The fixation system, in turn, replaces the three independently attached bone anchors. This limits the flexibility of the surgeon in choosing proper locations with sufficient bone thickness due to its predefined geometry. Therefore, the shape of the reference frame needs to consider the contribution of sufficiently thick regions at the lateral skull base and its variability between patients [37]. For the current design, we analyzed image data of 20 adult patient and averaged the identified regions suitable for safe and rigid bone-anchorage. However, further investigations with a larger sample size are necessary to determine what percentage of candidates can be treated with that one-size-fits-all Trifix.

Fixation of the reference frame is planned to be done through three small skin incisions as shown in Fig. 2 plus a fourth one for the drilling. Due to the early stage of development and its experimental character of this study, we went for a larger incision in most cases (Figs. 6(c) and 7). This enabled better access to the borehole for improved visualization and documentation in this study. The fixation was proved to be stable and rigid during the whole intervention in most cases. However, in two different cases (#07, #12) movements of the frame could be identified in the registered images (Sup. Fig. S5). Choosing more adequate screws for this application or developing a better fixation concept offers further room for improvements. In patients with very thick skin, the present length of the bone screws is too small. However, it needs further investigation whether specimen #04 represented a very rare condition and switching to the conventional approach is reasonable in these few cases or whether this will be the case in an appreciable amount of patients and demands for modifications of the Trifix's design.

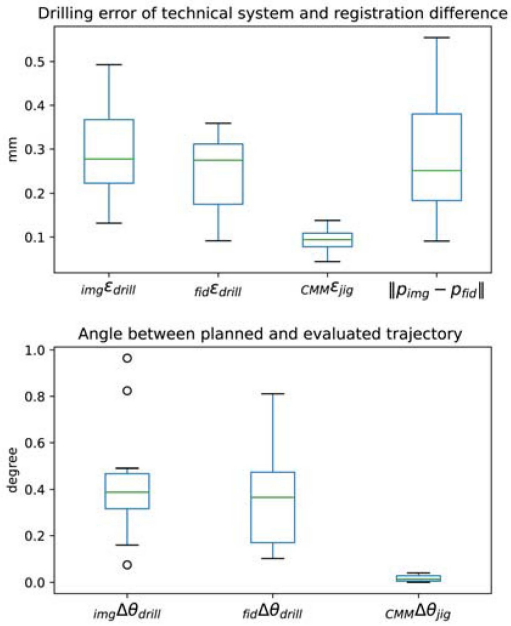

Fig. 8. Boxplots showing our different measurements of the drilling errors or components of this error measured radial to the planned path at the target depth in the middle ear. The lower plot displays the angular error. The manufactured individual drilling jigs can be measured very precisely with a coordinate measurement machine (CMM), so $_{CMM}\varepsilon_{jig}$ and $_{CMM}\Delta\theta_{jig}$ show that the jig contributes very little to the overall drilling error. The error estimated using image intensity based registration between the planning and the postoperative CBCT scan is denoted as $_{img}\varepsilon_{drill}$. The $_{fid}\varepsilon_{drill}$ is similar but uses fiducial based registration of the sphere markers attached to the MSF. The difference between image-based and fiducial-based registration as $\|p_{t,img} - p_{t,fid}\|$ hints at movements of the mini-stereotactic frame as the course for some of the (larger) errors.

Individualization of the jig was feasible in all cases. The proposed design of the manufacturing system could be proven as robust, practical, and reliable. Each blank could be customized in a single shot without need for repetition or rework resulting in a clean and true to size counterbore hole. As customization is reduced to drilling of only one hole and therefore only pressing the drill forward, operation of the device does not require special skills or training. The contribution of the customization step to the technical system accuracy, indicated by $_{CMM}\varepsilon_{jig}$, was determined with 0.09 mm $\pm$ 0.03 mm. This is in the same range as previously reported (0.11 mm $\pm$ 0.04 mm) [38].

Manual length setting of the hexapod's legs was identified as the most crucial step, which was shown to be error-prone. In two cases, operational errors resulted in jigs with deviations from the planning more than 4 times higher than during normal operation (Fig. 8). In a retrospective analysis we identified a mix-up of two digits as reason for this considerable maladjustment of the hexapod and therefore distinguish this type of inaccuracy (as caused by an extra-ordinary human error) from the technical

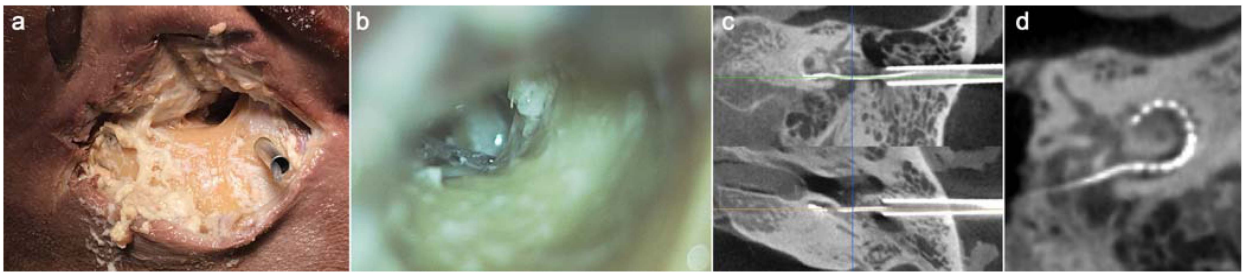

Fig. 9. (a) Drill canal with tube and electrode array inside. (b) Microscopic view through the external auditory canal showing the EA passing the tympanic cavity coming out of the drill canal (right) and entering the round window (left). (c) and (d) Post-experimental imaging confirming the intra-cochlear position of the EA.

accuracy of the system (which still includes small user errors due to human limitations in reading and adjusting the analog scale of the micrometer screws).

However, this source of error is the easiest to overcome. For the next iteration of the system, we are working on a fully automated manufacturing system so that human errors can be completely obviated.

The determined drilling accuracy of our system ($_{fid}\varepsilon_{drill} = 0.24\,\text{mm} \pm 0.09\,\text{mm}$; $_{img}\varepsilon_{drill} = 0.30\,\text{mm} \pm 0.11\,\text{mm}$; technical accuracy = without considerable human error) is comparable to the one of the HEARO system. Whose accuracy has been reported to be 0.21 mm ± 0.09 mm [13] with a worst case of 0.34 mm in in vivo experiments but at a lower drilling depth (facial recess). Our system accuracy was determined at the target point closer to the cochlea and is in the range suitable for cochlear implantation surgery as investigated in a previous study [39]. This value is also comparable to another micro-stereotactic frame (Microtable with 0.31 mm ± 0.10 mm) already used in a clinical investigation [33], [34].

In addition, this study provides useful insights and helped to identify several sources of errors which are going to be reduced in the future. This includes the registration markers as well as bone anchorage: Imaging of the frame and the spherical markers causes artifacts and therefore the distribution of fits vary higher in the direction of these artifacts. Especially in the region where the spheres are attached to the frame, they do not appear spherical (Sup. Fig. S2) which hampers manual selection. Manually selecting the spherical markers came on average with an uncertainty of approximately 0.1 mm, though substantial variability in precision has been seen during fitting of the model between individuals. This variability can be partly explained by different levels of experience with radiological image viewer. As errors in detection of the spherical markers during planning also impacts the total drilling accuracy, sphere markers that are easier to detect and an automated registration that would not only make the planning of the operation faster but also more secure. Although it is indisputable that there is room for further improvements in terms of automated marker detection and registration, our analysis of repeated selections of the both, spherical markers and rods, showed that it was possible to manually localize these structures with sub-voxel precision (approx. 0.1 mm vs. 0.3 mm voxel size).

Differences between $_{img}\varepsilon_{drill}$ and $_{fid}\varepsilon_{drill}$ can have different causes. In the scans without movement artifacts of the frame, the difference between sphere marker based registration and image registration were $\|p_{t,img} - p_{t,fid}\| = 0.21\,\text{mm} \pm 0.11\,\text{mm}$ and are most likely due to uncertainties in the determination of the location of the sphere markers. In cases #02 and # 05 imaged based registration was difficult due to movement artifacts in one of the CBCT scans, most likely due to a contact of the rotating scanner with the sterile drape covering the head and causing a slight movement of the skull inside the scan volume.

In the future, manufacturing of the jig could be performed under aseptic conditions according to the ISO 14644 family. Sterile blanks, drill bits, drapes and mounting platforms will be used in a controlled environment to maintain sterility of the blank respectively the jig. Therefore, no further sterilization of the produced jig will be required. In this preclinical trial using cadaveric specimens, sterile use was not yet implemented.

Insertion of the EA after drilling was beyond the scope of the present study. This subsequent step is only meaningful after sufficient accuracy of the micro-stereotactic procedure could be demonstrated, which was the primary aim of this study. However, we tested in two specimens the feasibility of electrode insertion into the cochlea using the minimally invasive access (Fig. 9). Only standard surgical instruments and a simple stainless-steel tube were used to push the electrode through the drill hole. A tympanomeatal flap was performed as an auxiliary access to the middle ear in order to guide the EA into the round window opening as no special insertion tool, as proposed elsewhere [40], [41], was utilized in these experiments. Full insertion of the Flex20 EA (MED-EL, Innsbruck, Austria) was possible in both specimens (Fig. 9(d)).

V. Conclusion

The presented results demonstrate the feasibility of the proposed micro-stereotactic procedure for performing a minimally invasive mastoidectomy with posterior tympanotomy approach as an important prerequisite for minimally invasive cochlear implantation surgery. The technology developed to fabricate an individualized jig itself provides sufficient accuracy. Manual adjustment of the fabrication system according to the individual planned trajectory, however, was identified as a potential source of user errors. For the future, we aim for an automated hexapod to ensure reliable safety for the patient.

Conflict of Interests

The authors TR, SJ, MK, OM, and TL declare being limited partners of HörSys IP GmbH & Co. KG that holds a financial stake in OtoJig GmbH. MF is employed by MED-EL Medical Electronics GmbH, which holds a financial stake in OtoJig GmbH. OtoJig is a German start-up that owns and further develops the described technology.

References

[1] F. Mueller et al., "Image-based planning of minimally traumatic inner ear access for robotic cochlear implantation," *Front. Surg.*, vol. 8, pp. 1–12, 2021, doi: 10.3389/fsurg.2021.761217.

[2] R. Torres et al., "Cochlear implant insertion axis into the basal turn: A critical factor in electrode array translocation," *Otology Neurotology*, vol. 39, no. 2, pp. 168–176, 2018.

[3] P. Aebischer et al., "In-vitro study of speed and alignment angle in cochlear implant electrode array insertions," *IEEE Trans. Biomed. Eng.*, vol. 69, no. 1, pp. 129–137, Jan. 2022.

[4] R. F. Labadie et al., "Minimally invasive, image-guided, facial-recess approach to the middle ear: Demonstration of the concept of percutaneous cochlear access in vitro," *Otology Neurotology*, vol. 26, no. 4, pp. 557–562, 2005, doi: 10.1097/01.mao.0000178117.61537.5b.

[5] A. Binnetoglu, B. Demir, and C. Batman, "Surgical complications of cochlear implantation: A 25-year retrospective analysis of cases in a tertiary academic center," *Eur. Arch. Oto-Rhino-Laryngology*, vol. 277, no. 7, pp. 1917–1923, 2020. [Online]. Available: https://doi.org/10.1007/s00405-020-05916-w

[6] S. Y. Kim et al., "Evaluating reasons for revision surgery and device failure rates in patients who underwent cochlear implantation surgery," *JAMA Otolaryngology - Head Neck Surg.*, vol. 146, no. 5, pp. 414–420, 2020, doi: 10.1001/jamaoto.2020.0030.

[7] O. Majdani et al., "A true minimally invasive approach for cochlear implantation: High accuracy in cranial base navigation through flat-panel-based volume computed tomography.," *Otology Neurotology*, vol. 29, no. 2, pp. 120–123, 2008, doi: 10.1097/mao.0b013e318157f7d8.

[8] F. M. Warren et al., "Percutaneous cochlear access using bone-mounted, customized drill guides: Demonstration of concept in vitro," *Otology Neurotology*, vol. 28, no. 3, pp. 325–329, 2007, doi: 10.1097/01.mao.0000253287.86737.2e.

[9] O. Majdani et al., "A robot-guided minimally invasive approach for cochlear implant surgery: Preliminary results of a temporal bone study," *Int. J. Comput. Assist. Radiol. Surg.*, vol. 4, no. 5, pp. 475–486, Sep. 2009, doi: 10.1007/s11548-009-0360-8.

[10] S. Baron et al., "Percutaneous inner-ear access via an image-guided industrial robot system," *Proc. Inst. Mech. Eng. Part H J. Eng. Med.*, vol. 224, no. 5, pp. 633–649, May 2010, doi: 10.1243/09544119JEIM781.

[11] L. B. Kratchman et al., "Design of a bone-attached parallel robot for percutaneous cochlear implantation," *IEEE Trans. Biomed. Eng.*, vol. 58, pp. 2904–2910, Oct. 2011, doi: 10.1109/TBME.2011.2162512.

[12] B. Bell et al., "A self-developed and constructed robot for minimally invasive cochlear implantation," *Acta Oto-Laryngologica*, vol. 132. pp. 355–360, 2012, doi: 10.3109/00016489.2011.642813.

[13] M. Caversaccio et al., "Robotic middle ear access for cochlear implantation: First in man," *PLoS One*, vol. 14, no. 8, pp. 1–12, 2019, doi: 10.1371/journal.pone.0220543.

[14] S. Weber et al., "Instrument flight to the inner ear," *Sci. Robot.*, vol. 2, no. 4, 2017, Art. no. eaal4916.

[15] R. F. Labadie et al., "Clinical validation of percutaneous cochlear implant surgery : Initial report," *Laryngoscope*, vol. 118, pp. 1031–1039, 2008.

[16] T. J. Ball et al., "Deep brain stimulation lead implantation using a customized rapidly manufactured stereotactic fixture with submillimetric euclidean accuracy," *Stereotactic Funct. Neurosurgery*, vol. 98, no. 4, pp. 248–255, 2020, doi: 10.1159/000506959.

[17] R. F. Labadie et al., "Customized, rapid-production microstereotactic table for surgical targeting: Description of concept and in vitro validation.," *Int. J. Comput. Assist. Radiol. Surg.*, vol. 4, no. 3, pp. 273–280, May 2009, doi: 10.1007/s11548-009-0292-3.

[18] R. Balachandran et al., "Percutaneous cochlear implant drilling via customized frames: An in vitro study," *Otolaryngology - Head Neck Surg.*, vol. 142, no. 3, pp. 421–426, 2010, doi: 10.1016/j.otohns.2009.11.029.

[19] D. A. Rajon et al., "Rapid fabrication of custom patient biopsy guides," *J. Appl. Clin. Med. Phys.*, vol. 10, no. 4, pp. 260–272, 2009, doi: 10.1120/jacmp.v10i4.2897.

[20] B. Vollmann et al., "Methods for intraoperative, sterile pose-setting of patient-specific microstereotactic frames," *Proc. SPIE*, vol. 9415, 2015, Art. no. 94150M, doi: 10.1117/12.2082066.

[21] J. P. Kobler et al., "Configuration optimization and experimental accuracy evaluation of a bone-attached, parallel robot for skull surgery," *Int. J. Comput. Assist. Radiol. Surg.*, vol. 11, no. 3, pp. 421–436, 2016, doi: 10.1007/s11548-015-1300-4.

[22] T. S. Rau et al., "Concept description and accuracy evaluation of a moldable surgical targeting system," *J. Med. Imag.*, vol. 8, no. 1, pp. 1–16, 2021, doi: 10.1117/1.jmi.8.1.015003.

[23] L. B. Kratchman and J. M. Fitzpatrick, "Robotically-adjustable microstereotactic frames for image-guided neurosurgery," *Proc. SPIE*, vol. 8671, no. 615, 2013, Art. no. 86711U, doi: 10.1117/12.2008172.

[24] R. Labadie et al., "Clinical validation study of percutaneous cochlear access using patient customized micro-stereotactic frames," *Otology Neurotology*, vol. 31, no. 1, pp. 94–99, 2010.

[25] T. S. Rau et al., "Preclinical evaluation of a micro-stereotactic surgical targeting system for minimally invasive cochlear implant surgery," in *Proc. 17th Annu. Meeting German Soc. Comput. Robot Assist. Surg.*, 2018, pp. 154–159.

[26] W. Thiel, "The preservation of the whole corpse with natural color (in German)," *Ann. Anat.*, vol. 174, no. 3, pp. 185–195, 1992.

[27] A. Fedorov et al., "3D Slicer as an image computing platform for the quantitative imaging network," *Magn. Reson. Imag.*, vol. 30, no. 9, pp. 1323–1341, 2012, doi: 10.1016/j.mri.2012.05.001.

[28] D. Stewart, "A platform with six degrees of freedom," *Proc. Inst. Mech. Eng.*, vol. 180, no. 1, pp. 371–386, 1965.

[29] T. Williamson et al., "Population statistics approach for safety assessment in robotic cochlear implantation," *Otology Neurotology*, vol. 38, pp. 759–764, 2017, doi: 10.1097/MAO.0000000000001357.

[30] C. R. Maurer et al., "Registration of head volume images using implantable fiducial markers," *IEEE Trans. Med. Imag.*, vol. 16, no. 4, pp. 447–462, Aug. 1997, doi: 10.1109/42.611354.

[31] G. Widmann et al., "Target registration and target positioning errors in computer-assisted neurosurgery: Proposal for a standardized reporting of error assessment," *Int. J. Med. Robot. Comput. Assist. Surg.*, vol. 5, no. 4, pp. 355–365, 2009.

[32] J. Kronenberg and L. Migirov, "The role of mastoidectomy in cochlear implant surgery," *Acta Otolaryngology*, vol. 123, no. 2, pp. 219–222, 2003, doi: 10.1080/0036554021000028112.

[33] R. F. Labadie et al., "Minimally invasive image-guided cochlear implantation surgery: First report of clinical implementation," *Laryngoscope*, vol. 124, no. 8, pp. 1915–1922, 2014, doi: 10.1002/lary.24520.

[34] R. F. Labadie et al., "Clinical implementation of Second-generation minimally invasive Image-guided cochlear implantation surgery," *Otology Neurotology*, vol. 42, no. 5, pp. 702–705, 2021, doi: 10.1097/MAO.0000000000003025.

[35] M. Caversaccio et al., "Robotic cochlear implantation: Surgical procedure and first clinical experience," *Acta Otolaryngology*, vol. 137, no. 4, pp. 447–454, 2017.

[36] O. Bradac et al., "Accuracy of varioguide frameless stereotactic system against frame-based stereotaxy: Prospective, randomized, single-center study," *World Neurosurg*, vol. 104, pp. 831–840, 2017, doi: 10.1016/j.wneu.2017.04.104.

[37] J. Lecoeur et al., "Variability of the temporal bone surface's topography: Implications for otologic surgery," in *Proc. Med. Imag. Image-Guided Procedures Robot. Interv. Model 83161B*, 2012, vol. 83161B, pp. 8316–8346, doi: 10.1117/12.911373.

[38] M. Kluge et al., "Investigation on the accuracy of the intra-operative fabrication device of the RoboJig (in German)," in *Proc. 16th Annu. Meeting German Soc. Comput. Robot Assist. Surg.*, Hannover, Germany, 2017, pp. 262–265.

[39] T. S. Rau et al., "Characterizing the size of the target region for atraumatic opening of the cochlea through the facial recess," *Comput. Med. Imag. Graph.*, vol. 77, no. 101655, pp. 1–14, 2019, doi: 10.1016/j.compmedimag.2019.101655.

[40] K. E. Riojas et al., "A new manual insertion tool for minimally invasive, image-guided cochlear implant surgery," in *Proc. Med. Imag. Image-Guided Procedures Robot. Interv. Model*, 2019, pp. 122–128, doi: 10.1117/12.2512471.

[41] T. S. Rau et al., "A simple tool to automate the insertion process in cochlear implant surgery," *Int. J. Comput. Assist. Radiol. Surg.*, vol. 15, no. 11, pp. 1931–1939, 2020, doi: 10.1007/s11548-020-02243-7.